Multiscale Simulations of Nonlinear Phenomena of Plasmas

R. Numata*

Graduate School of Simulation Studies, University of Hyogo,
7-1-28 Minatojima Minami-machi, Chuo-ku, Kobe, Hyogo 650-0047, Japan

Abstract

Multiscale hierarchy is intrinsic in collsionless plasmas, where various kinetic effects having their own scales play important roles. Gyrokinetics and the gyrokinetic code `AstroGK` are introduced to study multiscale phenomena in plasmas. An application of the gyrokinetic simulation using `AstroGK` to magnetic reconnection as an example of multiscale phenomenon is discussed.

1 Introduction

Plasmas observed in fusion experiments or in wide varieties of astrophysical situations such as the galaxy clusters, the interstellar medium, the solar corona, solar winds, the Earth's magnetosphere are typically in high temperature or in low density. Since collisions can be rare in such plasmas, deviations from thermal equilibrium can be maintained relatively long times. In thermally non-equilibrium plasmas, effects due to particle pictures of plasmas called kinetic effects play crucial roles on plasma dynamics. Examples of the kinetic effects include inertia of ions and electrons having intrinsic scales of inertial skin depths, and finite Larmor radius (FLR) effects of ions and electrons. These effects usually generate fine structures in velocity space, therefore enhance dissipations due to collisions even though collisionality is considered to be low.

Nonlinear phenomena in kinetic plasmas usually exhibit multiscale structures where various kinetic effects working at their intrinsic spatial scales are inter-related. The gyrokinetic approach is well-suited to study kinetic dynamics of plasmas. Gyrokinetics is a limit of kinetic model that describes the low-frequency dynamics of weakly collisional plasmas. It is derived by averaging the kinetic Vlasov-Landau equation and Maxwell's equation over the fast cyclotron motion, thus it omits the fast MHD waves, the cyclotron resonance, but retains FLR effects, and collisionless wave-particle interactions via the Landau resonance.

The theoretical foundation of gyrokinetics has been developed extensively over the past four decades, and gyrokinetics is now broadly employed for numerical studies of turbulence driven by microinstabilities in laboratory plasmas. It has also been recently recognized that the gyrokinetic approach is appropriate for the study of astrophysical plasmas. Taking

*E-mail: numata@sim.u-hyogo.ac.jp.

advantage of the knowledge and computational techniques developed in the simulation of turbulence in fusion plasmas, we have developed a gyrokinetic simulation code, `AstroGK` [1], specifically for the study of astrophysical problems and basic properties of plasmas.

In this paper, we first present our approach to study multiscale phenomena in plasmas: gyrokinetics and gyrokinetic simulation using `AstroGK`. `AstroGK` has already proven its usefullness in a number of studies. Among others, we show our recent result on the tearing instability as a typical example of multiscale phenomena in plasmas even though the result is still in preliminary linear stage.

2 Gyrokinetics and `AstroGK`

In this section, we present the gyrokinetic-Maxwell (GK-M) system of equations solved in `AstroGK`, and brief overview of the code.

We first assume that scale separations in space and time are well satisfied such that small fluctuations are locally embedded in a background plasma which is slowly varying spatially and temporally. We consider a temporally constant mean magnetic field $\boldsymbol{B}_0 = B_0\hat{\boldsymbol{b}}_0$. In the presence of a mean magnetic field, we can adopt the gyrokinetic ordering and average over the fast cyclotron motion to reduce the Vlasov–Maxwell equations to the GK-M equations; see Howes et al. [2] and Schekochihin et al. [3] for derivations of these equations expressly intended for the study of astrophysical plasmas. We also assume spatially uniform background for the sake of simplicity.

Under the gyrokinetic ordering, the distribution function of particles up to the first order is given by

$$f_s = \left(1 - \frac{q_s\phi}{T_{0s}}\right) f_{0s} + h_s, \tag{1}$$

where $s = \mathrm{i}, \mathrm{e}$ (stands for ions and electrons) is the species label, $f_{0s} = n_{0s}/(\sqrt{\pi}v_{\mathrm{th},s})^3 \exp(-v^2/v_{\mathrm{th},s}^2)$ is the zeroth-order, equilibrium Maxwellian distribution function. The first-order part of the distribution function is composed of the Boltzmann response term, and the gyro-center distribution function h_s defined in the gyro-center coordinate $(\boldsymbol{R}_s, \boldsymbol{V}_s)$ where the coordinate transform is given by

$$\boldsymbol{R}_s = \boldsymbol{r} + \frac{\boldsymbol{v}\times\hat{\boldsymbol{z}}}{\Omega_s}, \qquad\qquad \boldsymbol{V}_s = \boldsymbol{v}. \tag{2}$$

Upon averaging over the gyro-phase, the gyrokinetic equation evolves $h_s = h_s(X_s, Y_s, Z_s, V_{\parallel,s}, V_{\perp,s}, t)$:

$$\frac{\partial h_s}{\partial t} + V_{\parallel,s}\frac{\partial h_s}{\partial Z_s} + \frac{1}{B_0}\left\{\langle\chi\rangle_{\boldsymbol{R}_s}, h_s\right\} = \frac{q_s f_{0s}}{T_{0s}}\frac{\partial\langle\chi\rangle_{\boldsymbol{R}_s}}{\partial t} + C(h_s), \tag{3}$$

where parallel and perpendicular subscripts refer to directions with respect to the mean magnetic field. The gyrokinetic potential is given by $\chi = \phi - \boldsymbol{v}\cdot\boldsymbol{A}$, and the linear collision term is represented by $C(h_s)$. The angle bracket $\langle\,\cdot\,\rangle_{\boldsymbol{R}_s}$ denotes the gyro-average at fixed gyro-center coordinate $\boldsymbol{R}_s$:

$$\langle F(\boldsymbol{r})\rangle_{\boldsymbol{R}_s} = \frac{1}{2\pi}\oint F\left(\boldsymbol{R}_s + \frac{\boldsymbol{V}_s\times\hat{\boldsymbol{Z}}}{\Omega_s}\right)\mathrm{d}\Theta_s, \tag{4}$$

where $\boldsymbol{V}_s = (V_{\perp,s}, V_{\parallel,s}, \Theta_s)$. (The gyro-average at fixed particle coordinate $\langle\ \cdot\ \rangle_{\boldsymbol{r}}$ can also be defined by switching roles of $\boldsymbol{r}$ and $\boldsymbol{R}_s$.)

In the GK-M system, the electromagnetic fields are specified by the three scalar functions $\phi(\boldsymbol{r},t)$, $A_\parallel(\boldsymbol{r},t)$, and $\delta B_\parallel(\boldsymbol{r},t)$ [1] according to:

$$\boldsymbol{B} = \nabla_\perp A_\parallel \times \hat{\boldsymbol{z}} + \delta B_\parallel \hat{\boldsymbol{z}}, \qquad \boldsymbol{E} = -\nabla\phi - \frac{\partial \boldsymbol{A}}{\partial t}. \tag{5}$$

Maxwell's equations in the gyrokinetic limit reduce to the quasi-neutrality condition, and the parallel and perpendicular components of Ampère's law:

$$\sum_s \left[-\frac{q_s^2 n_{0s}}{T_{0s}}\phi + q_s \int \langle h_s \rangle_{\boldsymbol{r}} \mathrm{d}\boldsymbol{v} \right] = 0, \tag{6}$$

$$-\nabla_\perp^2 A_\parallel = \mu_0 \sum_s q_s \int \langle V_{\parallel,s} h_s \rangle_{\boldsymbol{r}} \mathrm{d}\boldsymbol{v}, \tag{7}$$

$$B_0 \nabla_\perp \delta B_\parallel = -\mu_0 \nabla_\perp \cdot \sum_s \int \langle m \boldsymbol{V}_{\perp,s} \boldsymbol{V}_{\perp,s} h_s \rangle_{\boldsymbol{r}} \mathrm{d}\boldsymbol{v}. \tag{8}$$

We refer the reader to [4] for the explicit form of the collision operator used in the code, as it has a rather cumbersome form. We mention here the basic properties of the operator. The operator is based on the linearized Landau collision operator transformed into the gyro-center coordinate. It has second-order velocity derivatives providing diffusion in velocity space and *conserving terms* which include integrations over velocity space. It is constructed to satisfy Boltzmann's *H*-theorem and the conservation of particles, momentum, and energy. It contains both like-species collisions and inter-species collisions, but the inter-species collisions account only for the collisions of electrons with one species of ions with large mass. Note that the linearized collision operator for a given species can be made independent of the first-order evolution of any other species. The theoretical basis of the collision operator is discussed in detail in [5].

`AstroGK` is a Eulerian initial value solver for the GK equation in five-dimensional phase space. It employs a pseudo-spectral algorithm to discretize the gyrokinetic equation in the spatial coordinates (x, y), an upwind finite-difference scheme in the z direction. Velocity space integrals in two dimensional velocity space are calculated using Gaussian quadrature rules. Time integration is made using the 3rd-order Adams-Bashforth for the nonlinear term. The linearized collision operator is treated by the first-order implicit Euler scheme with Sherman-Morrison formula for the moment-conserving corrections.

`AstroGK` is parallelized using MPI, and shows good parallel performance on various cutting edge supercomputers. Parallel performance is measured by taking the weak and strong scalings. The weak scaling is probed by holding the computational work per processing core constant while the number of cores, thus the total problem size, is increased. On the other hand, the strong scaling is probed by holding the problem size constant while the number of processing core is increased. Boths tests are performed on `Kraken` Cray XT5 system at the National Institute for Computational Sciences at the University of Tennessee. `Kraken`

[1] $\delta B_\parallel = (\nabla_\perp \times \boldsymbol{A}_\perp)_z$. We use the Coulomb gauge, which leads to $\nabla_\perp \cdot \boldsymbol{A}_\perp = 0$ with the ordering. Then, we can write $\boldsymbol{A}_\perp = \nabla_\perp \varsigma \times \hat{\boldsymbol{z}}$, and $\delta B_\parallel = -\nabla_\perp^2 \varsigma$ in terms of a single scalar function ς.

consists of 8256 computer nodes each having 12 processing cores, resulting in 99,072 compute cores in total.

Figure 1 shows the weak and strong scalings. From the weak scaling result, we observe that `AstroGK` follows the ideal scaling until the number of processors ($N_{\rm proc}$) equals to 12,288 with slight degradation of performance due to the increase of communication for $N_{\rm proc} > 1000$. From the strong scaling, we also observe the ideal scaling up to $N_{\rm proc} = 24,576$. Significant performance loss occurs only at $N_{\rm proc} = 49,152$.

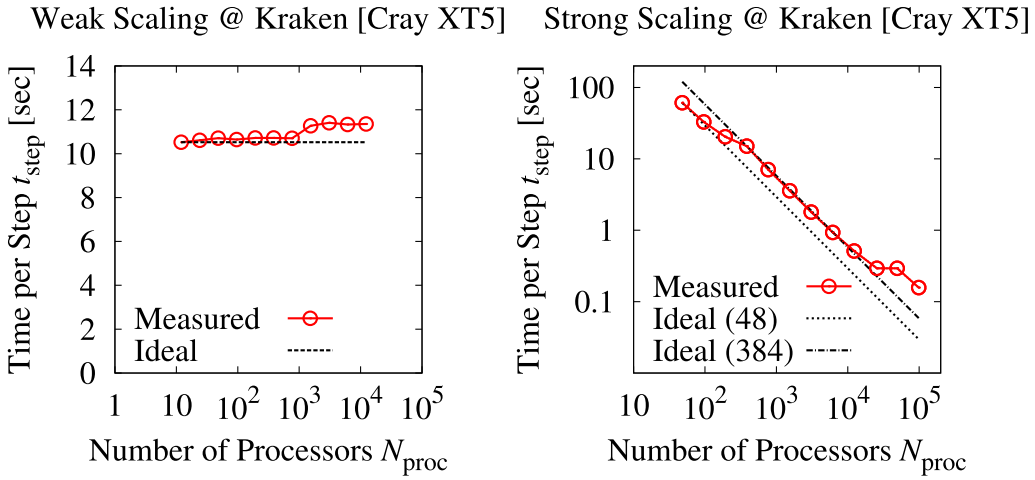

Figure 1: Parallel performance scaling of `AstroGK` on `Kraken` Cray XT5 system at NICS, the University of Tennessee. The left panel shows the weak scaling, and the right panel shows the strong scaling. Nearly ideal scalings are observed up to $10,000 \sim 20,000$ processors.

3 Magnetic reconnection as an example of multiscale phenomena

The tearing instability is important in magnetic fusion devices, where it drives the formation of magnetic islands that can significantly degrade heat and particle confinement. Solar flares and substorms in the Earth's magnetosphere are some of the many other contexts where tearing plays a crucial role, includeing magnetic reconncetion, explosive energy release, and large-scale reconfiguration of the magnetic field.

The evolusion of the tearing instability critically depends on the relationship between the width of the current layer, δ, where the frozen-flux condition breaks down and reconnection takes place, and the length scales characteristic of kinetic or non-magnetohydrodynamic (MHD) effects, such as the ion and electron skin-depth, $d_{\rm i}$ and $d_{\rm e}$, the ion sound Larmor radious, $\rho_{\rm Se}$, and the ion and electron Larmor radii, $\rho_{\rm i}$ and $\rho_{\rm e}$. For, sufficiently large electron-ion collision frequency, $\nu_{\rm e}$, the width of the reconnection layer well exceeds all of these non-MHD scales and the mode is expected to be well described by resistive MHD theory [6]. In many plasmas of interest, however, this is not the case: a decrease in the collisionality of the plasma leads to a decrease in the resistivity, causing the current layer width to shrink until

it reaches or falls below the largest relevant non-MHD scale.

3.1 Problem setup

We set up an initial sheared magnetic field

$$\boldsymbol{B} = B_0\hat{\boldsymbol{z}} + B_y^{\rm eq}(x)\hat{\boldsymbol{y}} \tag{9}$$

where B_0 is the background magnetic guide field and $B_y^{\rm eq}$ is the in-plane, reconnecting component. A super-imposed perturbation onto the equilibrium magnetic field will grow because of the tearing instability.

We scan in collisionality and use the Sptizer's formula to calculate the plasma resistivity η, recast in terms of the Lundquist number, $S = \mu_0 a V_{\rm A}/\eta = 2.63(\nu_{\rm e}\tau_{\rm A})^{-1}(d_{\rm e}/a)^{-2}$, where $V_{\rm A}$ is the Alfvén velocity corresponding to the peak value of $B_y^{\rm eq}$ and $\tau_{\rm A} \equiv a/V_{\rm A}$ is the Alfvén time. Other relevant quantities are:

$$\begin{aligned} \rho_{\rm i} &= \tau^{1/2}\rho_{\rm Se}\sqrt{2}, \quad d_{\rm i} = \beta_{\rm e}^{-1/2}\rho_{\rm Se}\sqrt{2}, \\ \rho_{\rm e} &= \sigma^{1/2}\rho_{\rm Se}\sqrt{2}, \quad d_{\rm e} = \beta_{\rm e}^{-1/2}\sigma^{1/2}\rho_{\rm Se}\sqrt{2}. \end{aligned} \tag{10}$$

$\sigma \equiv m_{\rm e}/m_{\rm i}$, $\tau \equiv T_{0\rm i}/T_{0\rm e}$, $\beta_{\rm e} \equiv n_0 T_{0\rm e}/(B_0^2/2\mu_0)$, $\rho_{\rm Se} \equiv c_{\rm Se}/\Omega_{\rm ci}$, $c_{\rm Se} = \sqrt{T_{0\rm e}/m_{\rm i}}$, $\Omega_{\rm ci} = eB_0/m_{\rm i}$. In addition to $\nu_{\rm e}$, the adjustable parameters considered here include the mass ratio σ, the electron beta $\beta_{\rm e}$, $\rho_{\rm Se}/a$, and τ, although the latter is held fixed at $\tau = 1$.

We study the collisional–collisionless transition by scanning in collisionality. As ν_e is decreased, the different ion and electron kinetic scales become important. Given the challenge of clearly separating all the relevant spatial scales in a kinetic simulation, we split our study into two sets of runs: a smaller-$\rho_{\rm Se}$ series ($\rho_{\rm Se}/a = 0.02/\sqrt{2} \simeq 0.014$) and a larger-$\rho_{\rm Se}$ series ($\rho_{\rm Se}/a = 0.2/\sqrt{2} \simeq 0.14$). Since $\tau = 1$ is held fixed, these two sets of runs also typically correspond to $\rho_{\rm i}/a = 0.02$ and $\rho_{\rm i}/a = 0.2$, respectively.

In the former set $\rho_{\rm e},\ d_{\rm e} \ll \rho_{\rm Se} \lesssim \delta \ll a$; in this case the frozen-flux condition is broken by collisions alone, and since δ well exceeds the collisionless electron scales $\rho_{\rm e},\ d_{\rm e}$, such scales need not be resolved in the simulations. The ion response, on the other hand, is predominantly collisional ($\delta > \rho_{\rm Se}$) at the smallest considered values of $S \sim 500$ but kinetic ($\delta \lesssim \rho_{\rm Se}$) at the largest values, $S \sim 10^5$. Thus resistive MHD would be expected, at least marginally, to be valid in this case at the smaller S values. In the set of runs with larger-$\rho_{\rm Se}$ ($\rho_{\rm Se}/a \simeq 0.14$), we again consider $\rho_{\rm e},\ d_{\rm e} \ll \rho_{\rm Se} \lesssim a$, but since $\rho_{\rm Se}/a$ is ten times larger than in the previous set of runs, the ions in this second set are predominantly kinetic ($\delta \lesssim \rho_{\rm Se}$) over the entire considered range of $S \sim 100 - 10^6$. Indeed, at the highest values of S, δ reaches collisionless electron scales ($d_{\rm e}$ at $\beta_{\rm e} \ll 1$ and $\rho_{\rm e}$ at $\beta_{\rm e} \sim 1$), and the instability dynamics become essentially collisionless.

In both sets of runs, we vary S over the ranges mentioned above for three different sets of $\beta_{\rm e}$ and $\sigma = m_e/m_i$: [($\beta_{\rm e}$, σ)=(0.3,0.01), (0.075,0.0025), (0.01875,0.000625)]. These parameters are such that $\rho_{\rm Se}/d_{\rm e} \equiv \sqrt{\beta_{\rm e}/(2\sigma)} = \sqrt{15} \simeq 3.9$ is held fixed and thus, since $\rho_{\rm Se}/a$ is also held fixed (at either 0.014 or 0.14), $d_{\rm e}/a$ is also held fixed (at either 0.0037 or 0.037, respectively). Given the parameter dependences of $d_{\rm i}$ and $\rho_{\rm e}$ noted in (10), however, it is seen that the values of $d_{\rm i}/a$ and $\rho_{\rm e}/a$ both change as $\beta_{\rm e}$ and σ are varied in this manner: for $\rho_{\rm Se} = 0.014$, $d_{\rm i} = 0.02/\sqrt{\beta_{\rm e}}$ and $\rho_{\rm e}/a = 0.02\sqrt{\sigma}$, while for $\rho_{\rm Se}/a = 0.14$ they are ten times larger.

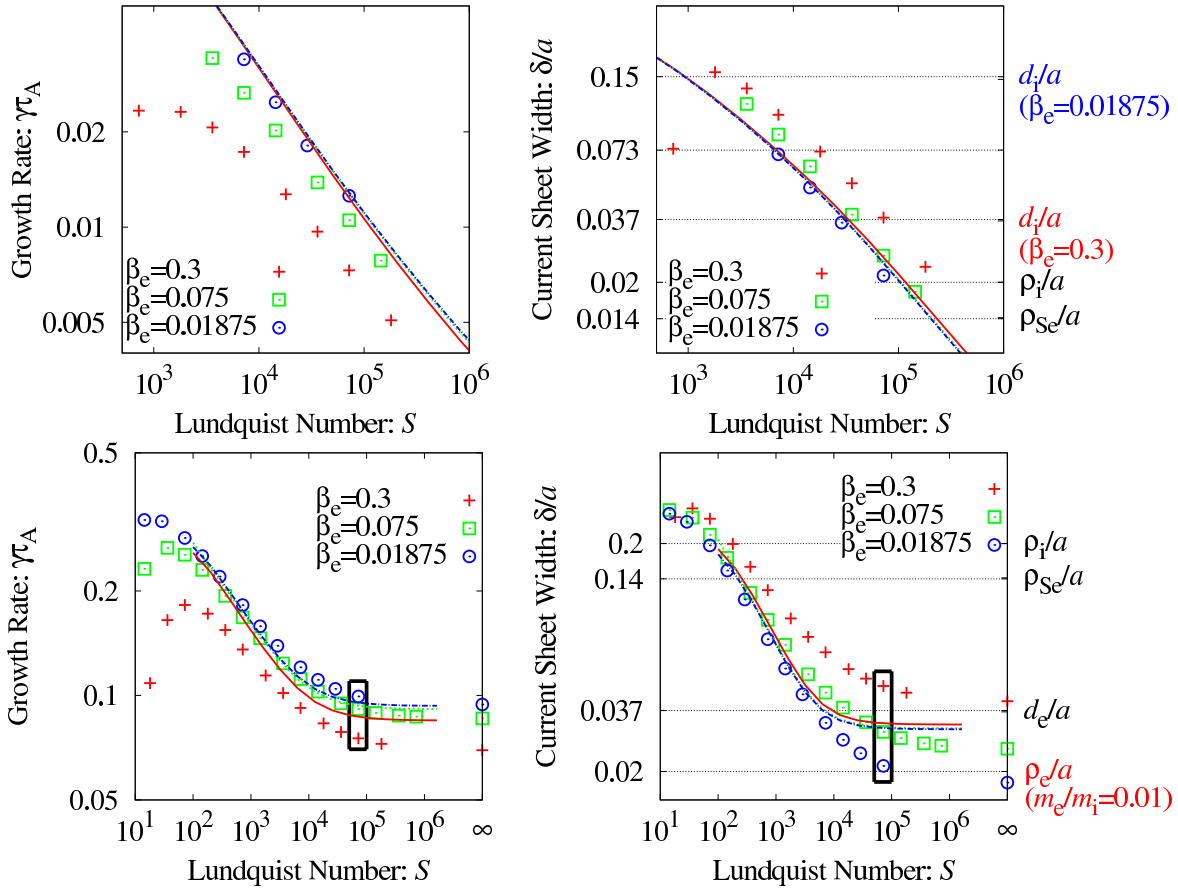

Figure 2: Growth rate and current sheet width versus the Lundquist number for $\rho_{\rm Se}/a = 0.02/\sqrt{2}$ (upper figures), and $\rho_{\rm Se}/a = 0.2/\sqrt{2}$ (lower figures). Red crosses, green squares, and blue circles show gyrokinetic results for $(\beta_{\rm e}, \sigma) = (0.3, 0.01), (0.075, 0.0025), (0.01875, 0.000625)$, respectively. Red solid, green dashed and blue dot-dashed lines are the corresponding two-fluid [7] scalings. The relevant scale lengths are identified on the right axis of the right panel.

3.2 Simulation results

Figure 2 shows the tearing mode growth rate ($\gamma = d\log A_\parallel/dt$ evaluated at the X-point) and current layer width (full-width at half-maximum) as functions of the Lundquist number (symbols) for $\tau = 1$. The upper panels correspond to $\rho_{\rm Se}/a = 0.014$, and the lower panels correspond to $\rho_{\rm Se}/a = 0.14$. Also plotted (lines) are the results obtained from a reduced two fluid model [7] with an isothermal electron equation of state. This model is derived under the assumption of low-$\beta_{\rm e}$, but exactly how low $\beta_{\rm e}$ must be for the validity of this model depends on how the various quantities in the model are ordered and is thus problem-dependent. For the ordering assumed in [7], it is argued that $\beta_{\rm e} \ll \sqrt{\sigma}$ is required — a condition that is marginally satisfied here only for the lowest $\beta_{\rm e}$ case, $(\beta_{\rm e}, \sigma) = (0.01875, 0.000625)$. The two fluid model is also derived under the assumption of cold ions, but the difference between the gyrokinetic results at $\tau = 0$ and $\tau = 1$ is small.

For the largest value of the collisionality, the gyrokinetic growth rates roll-over because the current layer width is too wide to satisfy the asymptotic scale separation, $\delta \ll a$, assumed in the two-fluid model tearing mode dispersion relation that is plotted in the figure. The deviation between the gyrokinetic and two-fluid results at the lowest S values should therefore be disregarded.

It is seen from the upper right panel that, as noted earlier, $\delta > \rho_{\rm Se}$ for all but the largest S values. In this case, as expected, the two-fluid model, at least at low-$\beta_{\rm e}$, recovers the well-known single-fluid resistive-MHD scalings [6] and is thus independent of $\beta_{\rm e}$. The over-estimation of the growth rates by the two fluid model at higher $\beta_{\rm e} \sim 0.3$ is possibly due to either a breakdown in the low-$\beta_{\rm e}$ ordering of the fluid model or a gradual onset of kinetic effects (e.g., the invalidity of a simple isothermal equation of state).

For the lower panels, we set $\rho_{\rm Se}/a = 0.14$, and adjust $\nu_{\rm e}$ such that $\delta \lesssim \rho_{\rm Se}$, thus focusing on the regime where ion kinetic effects are important. As in the previous case, we observe better agreement between the GK and two fluid results for lower values of $\beta_{\rm e}$. As S increases, the growth rate and the current layer width are less dependent on the collisionality. In this regime, electron kinetic effects (Landau damping and even finite electron orbits: note that for $\beta_{\rm e} = 0.3$, $\delta/\rho_{\rm e} \approx 2$) play an role to break the frozen-flux condition instead of collisions, thus called the collisionless regime. Since these effects are absent in the two fluid model, the scalings do not agree for any values of $\beta_{\rm e}$ in this regime.

4 Summary

Multiscale hierarchy is intrinsic in plasmas, and is observed in many situations of interest. In collisionless plasmas, various kinetic effects play important roles. Our approach to such multiscale phenomena is a gyrokinetic simulation. With the help of scale separation of dynamics under the mean magnetic field, we can reduce the phase space dimension from six to five using the gyrokinetic ordering, thus an accurate kinetic simulation becomes possible though it is still computational demanding.

We have briefly discussed the gyrokinetic model and the gyrokinetic simulation code, `AstroGK`, intended for studies of astrophysical plasmas and basic properties of plasmas. Then, we have shown the recent application of the gyrokinetic simulation to magnetic reconnection as a typical example of multiscale phenonema in plasmas. Starting from a collisional case, we gradually introduced various kinetic effect into the phenomena and observed transition from the collisional fluid-like case to the collisionless kinetic case by changing the collisionality parameter.

We have only shown one attempt of understanding multiscale phenomena in plasmas by the gyrokinetic simulation. However, there have been many studies of nonlinear gyrokinetic simulations using `AstroGK` published recent years. For example, the first kinetic simulations of turbulence describing the transition from Alfvén to kinetic Alfvén wave turbulence at the scale of the ion Larmor radius in an attempt to understand solar wind turbulence [8, 9], nonlinear phase-mixing properties of turbulence [10], the study of the statistical properties of phase-space structures of plasma turbulence [11], the Alfvén wave dynamics in the LAPD experiment [12]. We refer the readers to the listed publications for more detailed discussions.

Acknowlegement

The author would like to thank M. Barnes, W. Dorland, G. G. Howes, N. Loureiro, B. Rogers, and T. Tatsuno for fruitful collaborations.

References

[1] R. Numata, G. G. Howes, T. Tatsuno, M. Barnes, and W. Dorland, `AstroGK`: Astrophysical gryokinetics code, *J. Comput. Phys.* **229**, 9347 (2010).

[2] G. G. Howes, S. C. Cowley, W. Dorland, G. W. Hammett, E. Quataert, and A. A. Schekochihin, Astrophysical gyrokinetics: Basic equations and linear theory, *Astrophys. J.* **651**, 590 (2006).

[3] A. A. Schekochihin, S. C. Cowley, W. Dorland, G. W. Hammett, G. G. Howes, E. Quataert, and T. Tatsuno, Astrophysical gyrokinetics: Kinetic and fluid turbulent cascades in magnetized weakly collisional plasmas, *Astrophys. J. Suppl. Series* **182**, 310 (2009).

[4] M. Barnes, I. G. Abel, W. Dorland, D. R. Ernst, G. W. Hammett, P. Ricci, B. N. Rogers, A. A. Schekochihin, and T. Tatsuno, Linearized model Fokker-Planck collision operators for gyrokinetic simulations II. numerical implementation and tests, *Phys. Plasmas* **16**, 072107 (2009).

[5] I. G. Abel, M. Barnes, S. C. Cowley, W. Dorland, and A. A. Schekochihin, Linearized model Fokker-Planck collision operators for gyrokinetic simulations I. theory, *Phys. Plasmas* **15**, 122509 (2008).

[6] H. P. Furth, J. Killeen, and M. N. Rosenbluth, Finite-resistivity instabilities of a sheet pinch, *Phys. Fluids* **6**, 459 (1963).

[7] R. Fitzpatrick, Magnetic reconnection in weekly collisional highly magnetized electron-ion plasmas, *Phys. Plasmas* **17**, 042101 (2010).

[8] G. G. Howes, W. Dorland, S. C. Cowley, G. W. Hammett, E. Quataert, A. A. Schekochihin, and T. Tatsuno, Kinetic simulations of magnetized turbulence in astrophysical plasmas, *Phys. Rev. Lett.* **100**, 065004 (2008).

[9] G. G. Howes, J. M. TenBarge, W. Dorland, E. Quataert, A. A. Schekochihin, R. Numata, and T. Tatsuno, Gyrokinetic simulations of solar wind turbulence from ion to electron scales, *Phys. Rev. Lett.* **107**, 035004 (2011).

[10] T. Tatsuno, W. Dorland, A. A. Schekochihin, G. G. Plunk, M. Barnes, S. C. Cowley, and G. G. Howes, Nonlinear phase mixing and phase-space cascade of entropy in gyrokinetic plasma turbulence, *Phys. Rev. Lett.* **103**, 015003 (2009).

[11] T. Tatsuno, M. Barnes, S. C. Cowley, W. Dorland, G. G. Howes, R. Numata, G. G. Plunk, and A. A. Schekochihin, Gyrokinetic simulation of entropy cascade in two-dimensional electrostatic turbulence, *J. Plasma Fusion Res. SERIES* **9**, 509 (2010).

[12] K. D. Nielson, G. G. Howes, T. Tatsuno, R. Numata, and W. Dorland, Numerical modeling of Large Plasma Device Alfvén wave experiments using AstroGK, *Phys. Plasmas* **17**, 022105 (2010).